



Cite this: *Nanoscale*, 2019, **11**, 11107

Received 12th April 2019,

Accepted 26th May 2019

DOI: 10.1039/c9nr03162f

rsc.li/nanoscale

## Probing the interaction of nanoparticles with small molecules in real time *via* quartz crystal microbalance monitoring†

Ye Yang,<sup>a</sup> Guillaume Poss,<sup>b</sup> Yini Weng,<sup>a</sup> Runzhang Qi,<sup>a</sup> Hanrui Zheng,<sup>a</sup> Nikolaos Nianias,<sup>c</sup> Euan R. Kay<sup>b</sup> and Stefan Guldin<sup>\*,a</sup>

Despite extensive advances in the field of molecular recognition, the real-time monitoring of small molecule binding to nanoparticles (NP) remains a challenge. To this end, we report on a versatile approach, based on quartz crystal microbalance with dissipation monitoring, for the stepwise *in situ* quantification of gold nanoparticle (AuNPs) immobilisation and subsequent uptake and release of binding partners. AuNPs stabilised by thiol-bound ligand shells of prescribed chemical composition were densely immobilised onto gold surfaces *via* dithiol linkers. The boronate ester formation between salicylic acid derivatives in solution and boronic acids in the AuNP ligand shell was then studied in real time, revealing a drastic effect of both ligand architecture and Lewis base concentration on the interaction strength. The binding kinetics were analysed with frequency response modelling for a thorough comparison of binding parameters including relaxation time as well as association rate constant. The results directly mirror those from previously reported in-depth studies using nuclear magnetic resonance spectroscopy. By achieving quantitative characterisation of selective binding of analytes with molecular weight below 300 Da, this new method enables rapid, low cost, rational screening of AuNP candidates for molecular recognition.

### 1. Introduction

Besides offering highly controllable sizes, shapes and optical properties, gold nanoparticles (AuNPs) can be prepared with various surface functionalities for the selective interaction with antibodies, peptides, proteins, drugs and other small

molecules.<sup>1–6</sup> Thiol-based surface stabilisation provides a vast library of ligands with functional groups such as alcohols, carboxylic acids, amino acids, and anions/cations.<sup>7–9</sup> The self-assembly of ligand shells with biotic and abiotic molecules enables bottom-up morphology control at the nanoscale to study the structure–property–function interplay with biological entities.<sup>10–13</sup> In analogy to biomolecular recognition prevalent in many biological processes,<sup>14,15</sup> AuNPs have been developed for molecular recognition as well as drug delivery, alongside other synthetic supramolecular systems, such as nanocarriers and artificial molecular machines.<sup>16–18</sup>

The screening of the affinity and selectivity of specifically designed AuNP ligand shells towards molecular targets is essential for any of the above mentioned applications. A number of characterisation techniques have been developed based on different transduction principles, such as optical, acoustic and calorimetric read-out.<sup>19</sup> Molecular labelling, as often used in fluorescence and Raman-based spectroscopy, restricts the choice of materials and may also interfere with the target study.<sup>20</sup> A label-free alternative is based on surface plasmon resonance (SPR), which provides excellent sensitivity and responsiveness but the signal interference by non-specific binding often renders the analysis rather challenging.<sup>21,22</sup> Thermal calorimetry methods offer established routes for the determination of binding constants,<sup>23</sup> but limitations exist regarding their low throughput and the requirement of large sample quantities. A number of suitable methodologies based on nuclear magnetic resonance (NMR) spectroscopy have recently emerged to study NP–analyte interaction, including specifically designed diffusion filter and magnetisation transfer methods.<sup>24–27</sup> While it is meanwhile possible to verify detailed binding mechanisms and identify multiple analytes by NMR, challenges remain, such as the requirement for relatively high sample concentrations and the availability of a suitable instrumentation infrastructure.

Quartz crystal microbalance with dissipation monitoring (QCM-D) offers, in principle, a viable route for label-free monitoring of molecular adsorption at interfaces in real time.<sup>28–30</sup>

<sup>a</sup>Department of Chemical Engineering, University College London, Torrington Place, London, WC1E 7JE, UK. E-mail: s.guldin@ucl.ac.uk

<sup>b</sup>EaStCHEM School of Chemistry, University of St Andrews, St Andrews, KY16 9ST, UK

<sup>c</sup>Institute of Materials, École Polytechnique Fédérale de Lausanne (EPFL), Station 12, 1015 Lausanne, Switzerland

† Electronic supplementary information (ESI) available: Experimental details on synthetic procedures, sample preparation and characterisation techniques; further results on QCM-D characterisation. See DOI: 10.1039/C9NR03162F



The established relationship between the change in the resonant frequency and adsorbed wet-mass enables accurate quantification of binding events. QCM-D was successfully implemented to probe binding events of AuNPs with macromolecules, such as proteins, nucleic acids, lipid bilayers, bacteria as well as solvent vapours (in multilayers).<sup>31–36</sup> While it is possible to detect mass changes as low as  $1 \text{ ng cm}^{-2}$ , the detection of molecules with low molecular weight remains challenging, often caused by either an insufficient interfacial area (due to a low grafting density), limited binding affinity, or a combination of these factors.

One type of molecular interaction, that has been applied in a variety of NP-based recognition systems, is the binding of NP-bound boronic acids (BAs) with *cis*-diol containing biomolecules or other dihydroxy compounds such as catechols.<sup>37–40</sup> This dynamic covalent binding process results in the formation of NP-bound boronate esters.<sup>41,42</sup> Typically, boronate ester formation is most favourable in the presence of Lewis bases, and various strategies have been explored for achieving stable complexation at near-neutral pH values, including adding electron-withdrawing groups and intramolecular tetracoordinated B–N bonds (Wulff-type BAs).<sup>43–47</sup> Governed by similar principles, salicylic acids (SAs) and their derivatives also form boronate complexes.<sup>48</sup> Unlike aerobically unstable catechols, SAs have recently been identified as ideal oxidatively inert candidates for selective dynamic covalent interactions with BAs.<sup>48,49</sup> From measurements using  $^{19}\text{F}$  and  $^1\text{H}$  NMR spectroscopy, binding strength of SAs and catechols with BAs were found to be highly sensitive to experimental variables, including concentration of bases, as well as the molecular architecture of both BA ligands and their target binding partners.<sup>25,48</sup> It is therefore crucial to develop a comparative screening method with simplicity and versatility for the study of BA binding partners, including the more complex nucleosides, saccharides, glycans and glycoproteins, all of which are of significant biological relevance.<sup>43,50,51</sup>

Herein, we explore in a methodical case study the screening of BA ligands, binding partners and base concentration *via* multichannel QCM-D to establish a suitable characterisation route for the real-time monitoring of AuNP–analyte interaction. By stepwise immobilisation of AuNPs and subsequent exposure to binding partners, we validate the ability to characterise uptake and release of small molecular weight binding partners and report on binding equilibrium constants obtained for different molecular ligand architectures, small molecule binding partners and Lewis base concentrations.

## 2. Results and discussion

The overall experimental protocol of the QCM-D based methodology described herein is presented in Fig. 1 and consists of three major steps: (1) functionalisation of the QCM sensor surface by dithiols, (2) AuNP immobilisation, and (3) exposure to binding partners. In this study, two phenylboronic acid ligands were compared (PBA1 and PBA2 in Fig. 1). Electron-

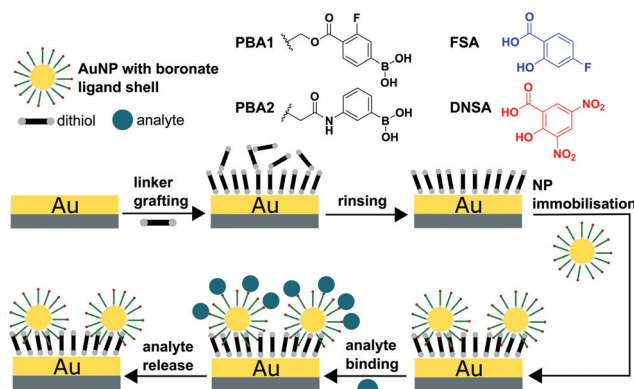


Fig. 1 Scheme of the QCM-D monitoring process and the molecular structure of PBAs and SAs used in this study.

withdrawing fluoro and carboxy ester substituents make PBA1 more Lewis acidic than PBA2, which bears an electron-donating amido group.<sup>48</sup> For oxidatively stable non-diol binding partners, 4-fluorosalicylic acid (FSA) and 3,5-dinitrosalicylic acid (DNSA) were assessed.<sup>48</sup>

Prior to the assessment of analyte binding, reusable QCM sensors were prepared by grafting monolayer stabilised AuNPs onto dithiol functionalised surfaces.<sup>52</sup> Fresh gold sensor surfaces (C2, C3 and C4) were first conditioned with methanol (MeOH) until stable baselines were obtained and offset for all overtones of frequency and dissipation. C2 and C3 were then exposed to 100 mM 1,8-octanedithiol (diOT) solutions in MeOH with subsequent rinsing by MeOH. C4 was used as control sample by flowing 10 mM MeOH solution of PBA1 in the disulfide form (dPBA1). As shown in Fig. 2(a), a decrease in frequency was observed with the flow of diOT, suggesting the attachment of the diOT molecules *via* gold–sulfur bonds. In comparison, the dissipation signal saw an increase during the process (Fig. S16<sup>†</sup>), which is likely attributed to a change in the bulk solution across the sensor surface. This is further supported by the fact that the dissipation shift returned to zero while the frequency shift stabilised at a certain level after rinsing with MeOH at  $100 \mu\text{L min}^{-1}$ , suggesting both the removal of the loosely attached diOT molecules but also the formation of a rigid layer on the sensor surface. The validity of the Sauerbrey equation allowed calculation of the areal mass (AM) change on the surface upon adsorption/desorption from the frequency shift (Fig. 2(b)).<sup>53</sup> With AM change at 137 and  $151 \text{ ng cm}^{-2}$  for C2 and C3, similar diOT grafting densities of 4.6 and  $5.1 \text{ per nm}^2$ , respectively, were achieved. Note that in comparison, the grafting of dPBA1 onto the sensor surface remained limited, with a mass change of  $20 \text{ ng cm}^{-2}$ .

Following the dithiol functionalisation step, the C2 and C3 sensors were then exposed to MeOH solutions of AuNPs ( $0.1 \text{ mg mL}^{-1}$ ) at a flow rate of  $10 \mu\text{L min}^{-1}$ . C2 was exposed to AuNPs capped with a homogeneous ligand layer of 11-mercapto-1-undecanol (MUO) (core size 3.7 nm in diameter) as a control, whilst PBA1-NPs (core size 3.6 nm in diameter) were flowed into C3. A significant decrease in frequency was



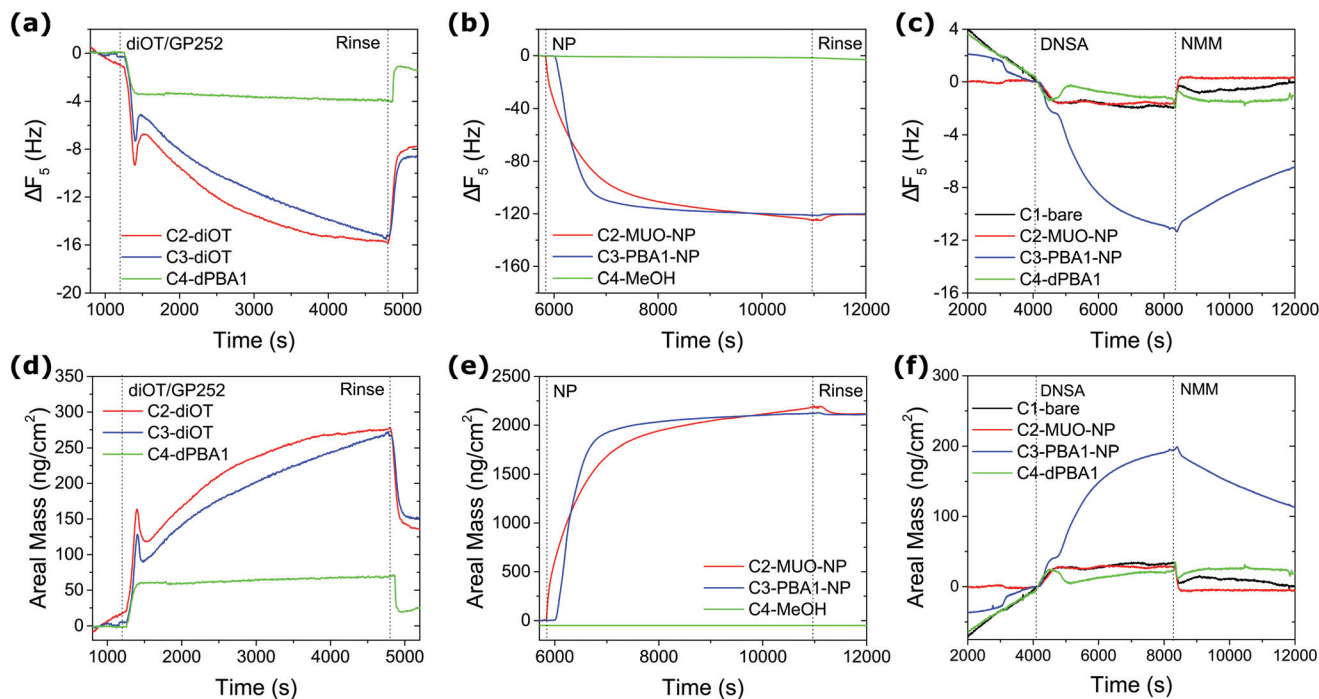


**Fig. 2** QCM monitoring of experimental procedure. Frequency shift and corresponding AM change ( $5^{\text{th}}$  overtone): (a, d) grafting of diOT onto gold surface; (b, e) immobilisation of AuNPs and (c, f) detection of 10 mM DNSA in MeOH with 10 mM NMM.

recorded for both channels during the first 15 min and no further adsorption was detected after 1 h constant flow (Fig. 2(c)). Notably, no desorption was observed after the MeOH rinsing step, suggesting the robust immobilisation of AuNPs, with AM change of 2120 and 2109  $\text{ng cm}^{-2}$  in each channel, respectively (Fig. 2(d)). This mass uptake is consistent with the formation of a densely packed layer of AuNPs. See ESI for calculation details (Tables S1 and S2†). Meanwhile, C4 control channel was flowed constantly with MeOH at flow rates matching those employed with C2 and C3; negligible background drift was observed. Whilst the AuNP immobilisation on Au surfaces builds on previous studies,<sup>54,55</sup> we note that the herein reported method promoted a significantly more efficient and robust AuNP grafting, which in return provides a larger interfacial area for assessment of AuNP-analyte interactions.

To assess the reactivity of the prepared sensor surface, 10 mM DNSA in 10 mM *N*-methylmorpholine (NMM) MeOH solution was introduced to the system after conditioning and equilibration with the buffer solution of 10 mM NMM in MeOH. As shown in Fig. 2(e) and (f), the adsorption of DNSA onto the sensor with PBA1-AuNPs (C3) led to a drastic frequency shift of 11 Hz and an AM change of 192  $\text{ng cm}^{-2}$ , compared to negligible changes for control sensors C1 (bare gold) and C4 (dPBA1), which can be attributed to physical adsorption and changes in the bulk environment. Significantly, no substantial frequency shift was observed for the C2 sensor with MUO-NPs, suggesting the signal observed for C3 is the result of a specific dynamic covalent interaction with the NP-

bound BAs. In approximation, the net AM change can be obtained by subtracting the contribution of non-specific physical adsorption and bulk solution obtained in control channels. Upon PBA-SA binding, the effective molecular weight of adsorbed species can be calculated as following:

$$MW_{\text{eff}} = MW_{\text{SA}} - 2MW_{\text{H}_2\text{O}} + MW_{\text{NMM}} \quad (1)$$

which takes into account the  $\text{H}_2\text{O}$  release and NMM association upon binding.<sup>48</sup> The density of bound DNSA on C3 was thus determined to be 2.75 per  $\text{nm}^2$ , showing a binding ratio of an average of 73 DNSA molecules per NP. This is particularly encouraging since there were approximately 156 PBA1 ligands on each PBA1-NP surface (Fig. S12 and S13†), with a significant proportion expected to be inaccessible on account of being orientated towards the sensor surface. We attribute this high binding ratio of 47%, in combination with the large interfacial area created by the high density AuNP surface grafting, to enable the monitoring of low molecular weight species, previously inaccessible by QCM-D.

The binding of two SAs (FSA or DNSA) to each of the PBA-functionalised NPs was assessed at three NMM base concentrations (0.05, 5 and 500 mM) in MeOH. Following the protocol described above, two sets of three fresh sensors were grafted with diOT and then immobilised with PBA1-NP or PBA2-NP, respectively. With the AM change for PBA1-NPs and PBA2-NPs measured at  $2077 \pm 38$  and  $1418 \pm 40$   $\text{ng cm}^{-2}$ , similar AuNP coverages were achieved for the sensors in the same group (Fig. S18–S21†). The grafting density of NP immobilisation as



well as PBA ligand density calculation is shown in Table S3.† AM change (Table 1) for each boronate ester complex was calculated from the recorded frequency shift (Fig. 3), evidencing a strong dependence on base concentration. At minimal base concentration (0.05 mM NMM), the frequency shift was largely subject to non-specific physical adsorption and bulk solution change. The negligible boronate ester formation confirmed the requirement of a basic environment for stabilising boronate ester complexes. Significantly improved binding affinity was observed for all four complexes when increasing the base concentration to a 1 : 1 molar ratio of NMM (5 mM) to binding partners. Meanwhile a reduced complex stability was observed at the higher NMM concentration of 500 mM, where the binding affinity for all four complexes was reduced compared to the values at 5 mM. These results are in direct agreement with studies of structurally analogous species in solution by quantitative NMR spectroscopy, which showed that a low base concentration (in the range of 1 : 1 molar ratio) was effective to induce strong boronate ester formation with SAs, contrary to the ultra-high concentrations (>100 molar equivalents) required to maximise binding with catechols.<sup>25,48</sup> In relation

to the low molecular weights of simple SAs, one limitation of the proposed platform is the detection at low concentrations by QCM-D, being a mass-based technique. The frequency shift of the 7<sup>th</sup> overtone was used for calculation to avoid noisy base-lines and we managed to assess the binding strength comfortably at analyte concentration of 5 mM with tolerable experimental errors. We anticipate the limit of detection to be further decreased by alternative binding partners of larger molecular weight.

To account for physical adsorption and bulk solution change for the estimation of the net AM change from boronate ester formation, the control baseline was carefully chosen as the AM change when flowing 5 mM FSA or DNSA repetition of 5 mM NMM on sensors immobilised with non-interacting MUO-NPs (Fig. S22†). The impact of NMM was compensated for by frequency and dissipation offset for individual measurement. The density of bound SAs was thus calculated, with the effective molecular weight  $MW_{\text{eff}}$  (from eqn (1)) for FSA and DNSA at 221.2 and 293.2 g mol<sup>-1</sup>, respectively (Table S4†). The binding ratios of bound SA to PBA receptors are summarised in Fig. 4. Direct comparison of the four complexes at 5 mM NMM reveals that PBA1-NP/FSA exhibited the strongest association under these conditions with a net binding of  $3.54 \pm 0.51$  FSA molecules per nm<sup>2</sup>, corresponding to 61% of the surface-immobilised BAs. The quantitative binding is consistent with results from NMR studies on closely analogous model compounds.<sup>48</sup> Also in line with solution-phase studies is the observation of weaker association exhibited by PBA2 complexes compared to each analogous PBA1 complex, which is a consequence of the lower Lewis acidity at the boron of PBA2.<sup>44,48,56,57</sup> Under the same conditions, PBA1-NP/DNSA achieved a 32% binding ratio (falling to 8% for PBA2-NP/DNSA). For acidic binding partners such as SAs, boronate complex formation is maximised at an optimal concentration of base. Each of the complexes studied exhibited reduced stability at the high base concentration of 500 mM, with the more acidic DNSA binding partner most severely affected. Once more, this reflects the behaviour expected on the basis of solution-phase studies.<sup>48,56,57</sup>

When rinsing with NMM MeOH solution, the release of both SAs was observed, resulting from the dissociation of the boronate esters, thus proving the reversible nature of this

**Table 1** Absolute AM change at varying experimental conditions

Sensor type	AM change, ng cm <sup>-2</sup>		
	Conc. NMM, mM		
	0.05	5	500
PBA1-NP/FSA	44	163	97
PBA1-NP/DNSA	20	102	36
PBA2-NP/FSA	32	103	88
PBA2-NP/DNSA	20	37	21

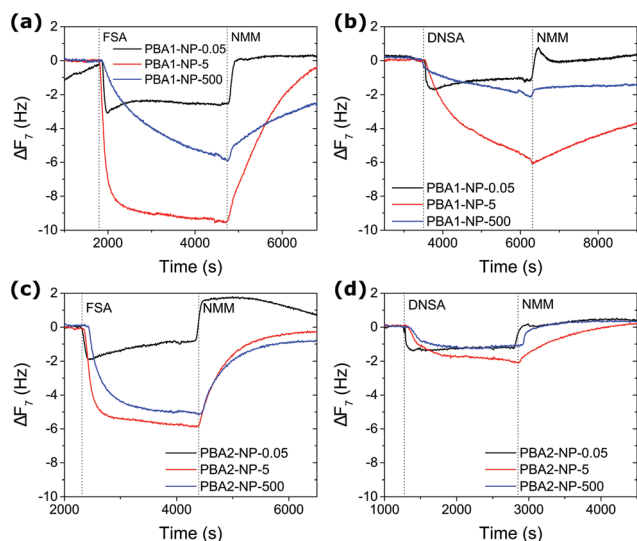


**Fig. 3** Variable screening of PBA-AuNP and SA binding. Frequency shift (7<sup>th</sup> overtone) at NMM base concentration of 0.05, 5 and 500 mM: PBA1-NPs with 5 mM of (a) FSA and (b) DNSA; PBA2-NPs with 5 mM of (c) FSA and (d) DNSA.

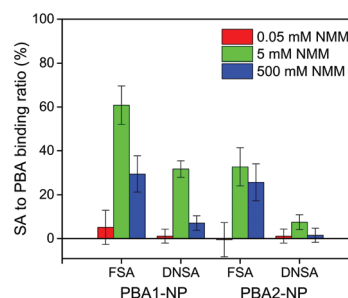


**Fig. 4** Binding ratio of SA to PBA calculated from net AM change of 5 mM SA at 0.05, 5 and 500 mM NMM. The error estimation is based on control subtraction and sensor ligand density variation.



dynamic covalent condensation–hydrolysis reaction.<sup>43</sup> After extended washing for 1 h, all pre-bound SA molecules were released as indicated by the net frequency shift returning to the same resonant frequency as during NMM MeOH equilibration (Fig. S23 and S24†). Quantitative information on the binding kinetics of boronate ester formation can be assessed by mass change over time with following equations:<sup>58–60</sup>



$$\Delta m_t = \Delta m_{\text{max}}(1 - e^{-t/\tau}) \quad (3)$$

$$\tau^{-1} = k_{\text{on}} \times [\text{SA}] + k_{\text{off}} \quad (4)$$

where  $k_{\text{on}}$  and  $k_{\text{off}}$  are the association and dissociation rate constants,  $\Delta m_{\text{max}}$  is the maximum mass change and  $\tau$  is the relaxation time.

During rinsing, in particular,  $[\text{SA}] = 0$ , eqn (3) can be written as following:

$$\tau_{\text{off}}^{-1} = k_{\text{off}}. \quad (5)$$

Therefore, the apparent binding constant  $K_a$  can be calculated from following equation:

$$K_a = \frac{k_{\text{on}}}{k_{\text{off}}} = \frac{\tau_{\text{on}}^{-1} - \tau_{\text{off}}^{-1}}{[\text{SA}] \times \tau_{\text{off}}^{-1}}. \quad (6)$$

With local fitting of the dissociation and then the association process, the binding parameters for the experiments at 5 and 500 mM NMM solutions were modelled with exponential decay function as detailed in eqn (3). The obtained relaxation time  $\tau$  for both association and dissociation was used to calculate association and dissociation rate constants ( $k_{\text{on}}$  and  $k_{\text{off}}$ ) as well as apparent binding constant  $K_a$ . The fitting curves are shown in Fig. S25† and fitting results are summarised in Table 2. On top of the kinetic information provided by  $\tau$  values, the binding constants further evidenced the observed effects of NMM concentration as well as the structure of both PBA and SA components. Boronate complex stability depends on the structure of each binding partner, as well as the concentration of base. The absolute complex stability, optimum base

concentration, and sensitivity to changes away from these conditions all depend on the relative and absolute acidities of the two binding partners. To fully map this multi-dimensional variable space and optimise boronate complex formation, traditional methods such as NMR spectroscopy present a significantly time-consuming and costly challenge, which becomes even greater when examining NP-bound systems. Furthermore, it is not commonly possible to extract information on binding kinetics for such labile molecular interactions from NMR studies. Potentiometric methods have traditionally been used to characterise these aspects of boronate esters, however such approaches are non-trivial to apply to NP systems and are not well-suited to studies in non-aqueous solvents. By contrast, analysis by QCM-D is intrinsically surface based, with reusable AuNP-grafted sensor surfaces that are readily reactivated simply by extended washing. QCM-D thus presents a parallel and sample-efficient method for rapid screening and optimising complex formation for variations in both structural and experimental variables, while at the same time extracting detailed kinetic and thermodynamic information.

### 3. Conclusions

In conclusion, we demonstrate an effective route to study NP–analyte surface interactions in real time using a multichannel QCM-D platform. The method consists of essentially three steps, namely the functionalisation of gold coated quartz crystals with dithiol linkers, the grafting of thiol-stabilised AuNPs with functional end groups and the exposure to the binding partners of interest. We employ this approach for the study of boronate ester formation induced by the binding of SAs to AuNPs with BA ligands. Both variables, the molecular architecture of the BA ligands and the concentration of Lewis bases, led to significant changes to the equilibrium binding ratio. Furthermore, the frequency shift pattern was used to model the kinetics during association and dissociation events. Important information including relaxation time as well association/dissociation rate constants could be calculated from this detailed analysis. In contrast to previous QCM-D studies focusing on macromolecules in the kDa molecular weight range or the use of NPs as signal amplification labels, we were able to resolve frequency shifts induced by the binding of immobilised AuNPs to analytes in solution, with molecular weight as low as 100–300 Da. This represents an ideal characterisation platform for the rational screening and selection of AuNP candidates for molecular recognition, adding unique opportunities to the existing tool box for AuNP–analyte interaction.

### 4. Experimental section

#### 4.1. AuNP preparation

The preparation and characterisation of PBA ligands as well as PBA–NPs were detailed in ESI.† MUO–AuNPs were prepared *via*

**Table 2** Apparent binding parameters calculated from AM change of 5 mM SA at 5 and 500 mM NMM

Sensor type	Binding parameters			
	$\tau_{\text{off}}^{-1}$ $10^{-3} \text{ s}^{-1}$	$\tau_{\text{on}}^{-1}$ $10^{-3} \text{ s}^{-1}$	$k_{\text{on}}$ $\text{s}^{-1} \text{ M}^{-1}$	$K_a$ $10^6 \text{ M}^{-1}$
<b>5 mM NMM</b>				
PBA1-NP/FSA	0.82	8.25	1487.2	1.82
PBA1-NP/DNSA	0.20	1.27	213.7	1.06
PBA2-NP/FSA	2.29	7.89	1121.6	0.49
PBA2-NP/DNSA	1.39	4.49	620.8	0.45
<b>500 mM NMM</b>				
PBA1-NP/FSA	0.62	1.17	110.4	0.18
PBA1-NP/DNSA	1.52	2.49	194.6	0.13
PBA2-NP/FSA	2.42	4.23	360.5	0.15
PBA2-NP/DNSA	4.10	5.94	368.4	0.09



the oleylamine ligand-exchange approach. The synthesis and characterisation have been previously reported.<sup>61</sup>

#### 4.2. QCM-D

All QCM-D studies were performed with 4.95 MHz AT-cut gold coated quartz Qsensors on a QSense QCM-D Analyser (Biolin Scientific, Sweden) coupled with an Ismatec IPC-N 4 peristaltic pump. Fresh sensors were rinsed with ethanol and dried with N<sub>2</sub> before installing into the flow module. All QCM-D experiments were measured at a controlled temperature of 20 °C. Different flow rates were used with 200 μl min<sup>-1</sup> for MeOH, 100 μl min<sup>-1</sup> for NMM buffer, 10 μl min<sup>-1</sup> for thiols, AuNPs and binding partners. The data was collected and analysed with QSoft 401 and QTools 301 softwares developed by Biolin Scientific. The areal mass change data was calculated based on the Sauerbrey equation<sup>62</sup> as follows:

$$\Delta m = -C \times \Delta f_n \quad (7)$$

$$\Delta f_n = \frac{\Delta f_n^{\text{Abs}}}{n} \quad (8)$$

where  $\Delta m$  is the mass change per unit area,  $C$  is a constant which is equal to 17.5 ng (cm<sup>2</sup> Hz)<sup>-1</sup> for 4.95 MHz Qsensors,  $\Delta f_n^{\text{Abs}}$  is the frequency shift of  $n^{\text{th}}$  overtone and  $n$  is the overtone number.

## Conflicts of interest

There are no conflicts to declare.

## Acknowledgements

Y. Y. acknowledges University College London (UCL) for the Overseas Research Scholarship and the Graduate Research Scholarship. The project received funding from the European Unions Horizon 2020 research and innovation programme under grant agreement no. 633635 (DIACHEMO) and the EPSRC (grant number EP/J500549/1). Mass spectrometry was carried out at the UK National Mass Spectrometry Facility (NMSF) at Swansea University. The authors are grateful to Jugal Suthar (UCL) for providing valuable feedback on the manuscript.

## References

- M.-C. Daniel and D. Astruc, *Chem. Rev.*, 2004, **104**, 293–346.
- Y.-C. Yeh, B. Creran and V. M. Rotello, *Nanoscale*, 2012, **4**, 1871–1880.
- R. Wilson, *Chem. Soc. Rev.*, 2008, **37**, 2028–2045.
- P. D. Howes, R. Chandrawati and M. M. Stevens, *Science*, 2014, **346**, 1247390.
- V. Montes-García, J. Pérez-Juste, I. Pastoriza-Santos and L. M. Liz-Marzán, *Chem. – Eur. J.*, 2014, **20**, 10874–10883.
- F. Scaletti, J. Hardie, Y.-W. Lee, D. C. Luther, M. Ray and V. M. Rotello, *Chem. Soc. Rev.*, 2018, **47**, 3421–3432.
- V. Biju, *Chem. Soc. Rev.*, 2014, **43**, 744–764.
- R. A. Sperling and W. J. Parak, *Philos. Trans. R. Soc., A*, 2010, **368**, 1333–1383.
- S. Engel, E.-C. Fritz and B. J. Ravoo, *Chem. Soc. Rev.*, 2017, **46**, 2057–2075.
- Q. Mu, G. Jiang, L. Chen, H. Zhou, D. Fourches, A. Tropsha and B. Yan, *Chem. Rev.*, 2014, **114**, 7740–7781.
- A. E. Nel, L. Mädler, D. Velegol, T. Xia, E. M. Hoek, P. Somasundaran, F. Klaessig, V. Castranova and M. Thompson, *Nat. Mater.*, 2009, **8**, 543.
- M. P. Monopoli, C. Åberg, A. Salvati and K. A. Dawson, *Nat. Nanotechnol.*, 2012, **7**, 779.
- D. Docter, D. Westmeier, M. Markiewicz, S. Stolte, S. Knauer and R. Stauber, *Chem. Soc. Rev.*, 2015, **44**, 6094–6121.
- J.-M. Lehn, *Angew. Chem., Int. Ed. Engl.*, 1990, **29**, 1304–1319.
- G. Yu, K. Jie and F. Huang, *Chem. Rev.*, 2015, **115**, 7240–7303.
- G. Raschke, S. Kowarik, T. Franzl, C. Sönnichsen, T. Klar, J. Feldmann, A. Nichtl and K. Kürzinger, *Nano Lett.*, 2003, **3**, 935–938.
- S. M. Simoes, A. Rey-Rico, A. Concheiro and C. Alvarez-Lorenzo, *ChemComm*, 2015, **51**, 6275–6289.
- H. Yang, B. Yuan, X. Zhang and O. A. Scherman, *Acc. Chem. Res.*, 2014, **47**, 2106–2115.
- M. A. Cooper, *Anal. Bioanal. Chem.*, 2003, **377**, 834–842.
- S. Ray, G. Mehta and S. Srivastava, *Proteomics*, 2010, **10**, 731–748.
- H. Im, H. Shao, Y. I. Park, V. M. Peterson, C. M. Castro, R. Weissleder and H. Lee, *Nat. Biotechnol.*, 2014, **32**, 490.
- H. H. Nguyen, J. Park, S. Kang and M. Kim, *Sensors*, 2015, **15**, 10481–10510.
- R. Huang, R. P. Carney, F. Stellacci and B. L. Lau, *Nanoscale*, 2013, **5**, 6928–6935.
- B. Perrone, S. Springhetti, F. Ramadori, F. Rastrelli and F. Mancin, *J. Am. Chem. Soc.*, 2013, **135**, 11768–11771.
- S. Borsley and E. R. Kay, *Chem. Commun.*, 2016, **52**, 9117–9120.
- L. Gabrielli, D. Rosa-Gastaldo, M.-V. Salvia, S. Springhetti, F. Rastrelli and F. Mancin, *Chem. Sci.*, 2018, **9**, 4777–4784.
- G. Salassa and T. Bürgi, *Nanoscale Horiz.*, 2018, **3**, 457–463.
- M. Nirschl, F. Reuter and J. Vörös, *Biosensors*, 2011, **1**, 70–92.
- R. P. Richter, R. Bérat and A. R. Brisson, *Langmuir*, 2006, **22**, 3497–3505.
- G. V. Dubacheva, C. Araya-Callis, A. Geert Volbeda, M. Fairhead, J. Codée, M. Howarth and R. P. Richter, *J. Am. Chem. Soc.*, 2017, **139**, 4157–4167.
- S. H. Brewer, W. R. Glomm, M. C. Johnson, M. K. Knag and S. Franzen, *Langmuir*, 2005, **21**, 9303–9307.
- B. Tajik-Ahmadabad, A. Mechler, B. W. Muir, K. McLean, T. M. Hinton, F. Separovic and A. Polyzos, *ChemBioChem*, 2017, **18**, 921–930.



- 33 C. M. Bailey, E. Kamaloo, K. L. Waterman, K. F. Wang, R. Nagarajan and T. A. Camesano, *Biophys. Chem.*, 2015, **203**, 51–61.
- 34 F. Salam, Y. Uludag and I. E. Tothill, *Talanta*, 2013, **115**, 761–767.
- 35 R. C. Van Lehn, M. Ricci, P. H. Silva, P. Andreozzi, J. Reguera, K. Voitchovsky, F. Stellacci and A. Alexander-Katz, *Nat. Commun.*, 2014, **5**, 4482.
- 36 Z. M. Marsh, K. A. Lantz and M. Stefik, *Nanoscale*, 2018, **10**, 19107–19116.
- 37 N. Kanayama and H. Kitano, *Langmuir*, 2000, **16**, 577–583.
- 38 W. Zhou, N. Yao, G. Yao, C. Deng, X. Zhang and P. Yang, *Chem. Commun.*, 2008, 5577–5579.
- 39 J. Liu, K. Yang, Y. Qu, S. Li, Q. Wu, Z. Liang, L. Zhang and Y. Zhang, *Chem. Commun.*, 2015, **51**, 3896–3898.
- 40 L. Liang and Z. Liu, *Chem. Commun.*, 2011, **47**, 2255–2257.
- 41 J. P. Lorand and J. O. Edwards, *J. Org. Chem.*, 1959, **24**, 769–774.
- 42 R. Pizer and L. Babcock, *Inorg. Chem.*, 1977, **16**, 1677–1681.
- 43 X. Wu, Z. Li, X.-X. Chen, J. S. Fossey, T. D. James and Y.-B. Jiang, *Chem. Soc. Rev.*, 2013, **42**, 8032–8048.
- 44 J. Yan, G. Springsteen, S. Deeter and B. Wang, *Tetrahedron*, 2004, **60**, 11205–11209.
- 45 L. Zhu, S. H. Shabbir, M. Gray, V. M. Lynch, S. Sorey and E. V. Anslyn, *J. Am. Chem. Soc.*, 2006, **128**, 1222–1232.
- 46 G. Wulff, *Pure Appl. Chem.*, 1982, **54**, 2093–2102.
- 47 M. Dowlut and D. G. Hall, *J. Am. Chem. Soc.*, 2006, **128**, 4226–4227.
- 48 S. Borsley, G. Poss, R. L. Spicer, E. Boudin and E. R. Kay, *Supramol. Chem.*, 2018, **30**, 772–781.
- 49 M. Arzt, C. Seidler, D. Y. Ng and T. Weil, *Chem. – Asian J.*, 2014, **9**, 1994–2003.
- 50 R. Nishiyabu, Y. Kubo, T. D. James and J. S. Fossey, *Chem. Commun.*, 2011, **47**, 1106–1123.
- 51 D. Li, Y. Chen and Z. Liu, *Chem. Soc. Rev.*, 2015, **44**, 8097–8123.
- 52 M. Brust, R. Etchenique, E. Calvo and G. Gordillo, *Chem. Commun.*, 1996, 1949–1950.
- 53 M. Rodahl, F. Höök, C. Fredriksson, C. A. Keller, A. Krozer, P. Brzezinski, M. Voinova and B. Kasemo, *Faraday Discuss.*, 1997, **107**, 229–246.
- 54 L. Lin, H.-q. Zhao, J.-r. Li, J.-a. Tang, M.-x. Duan and L. Jiang, *Biochem. Biophys. Res. Commun.*, 2000, **274**, 817–820.
- 55 X. Li, Y. Yasutake, K. Kono, M. Kanehara, T. Teranishi and Y. Majima, *Jpn. J. Appl. Phys.*, 2009, **48**, 04C180.
- 56 M. A. Martinez-Aguirre, R. Villamil-Ramos, J. A. Guerrero-Alvarez and A. K. Yatsimirsky, *J. Org. Chem.*, 2013, **78**, 4674–4684.
- 57 Y. Furikado, T. Nagahata, T. Okamoto, T. Sugaya, S. Iwatsuki, M. Inamo, H. D. Takagi, A. Odani and K. Ishihara, *Chem. – Eur. J.*, 2014, **20**, 13194–13202.
- 58 Y. Ebara and Y. Okahata, *J. Am. Chem. Soc.*, 1994, **116**, 11209–11212.
- 59 Y. Okahata, M. Kawase, K. Niikura, F. Ohtake, H. Furusawa and Y. Ebara, *Anal. Chem.*, 1998, **70**, 1288–1296.
- 60 X. Turon, O. J. Rojas and R. S. Deinhammer, *Langmuir*, 2008, **24**, 3880–3887.
- 61 Y. Yang, L. A. Serrano González and S. Guldin, *Langmuir*, 2018, **34**, 6820–6826.
- 62 G. Sauerbrey, *Z. Phys.*, 1959, **155**, 206–222.

